We are IntechOpen, the world's leading publisher of Open Access books Built by scientists, for scientists

6,900
Open access books available

185,000
International authors and editors

200M
Downloads

Our authors are among the

154
Countries delivered to

TOP 1%
most cited scientists

12.2%
Contributors from top 500 universities



WEB OF SCIENCE™

Selection of our books indexed in the Book Citation Index in Web of Science™ Core Collection (BKCI)

Interested in publishing with us?
Contact book.department@intechopen.com

Numbers displayed above are based on latest data collected.
For more information visit www.intechopen.com



21

MAP Classification of a Reference Image Using Auxiliaries Images with Different Prevalent Classes

[1,2]Orlando Alves Máximo and [2]David Fernandes
[1]*Instituto de Estudos Avançados (IEAv)-Comando- Geral de Tecnologia Aeroespacial*
[2]*Instituto Tecnológico de Aeronáutica (ITA)-Comando -Geral de Tecnologia Aeroespacial*
Brazil

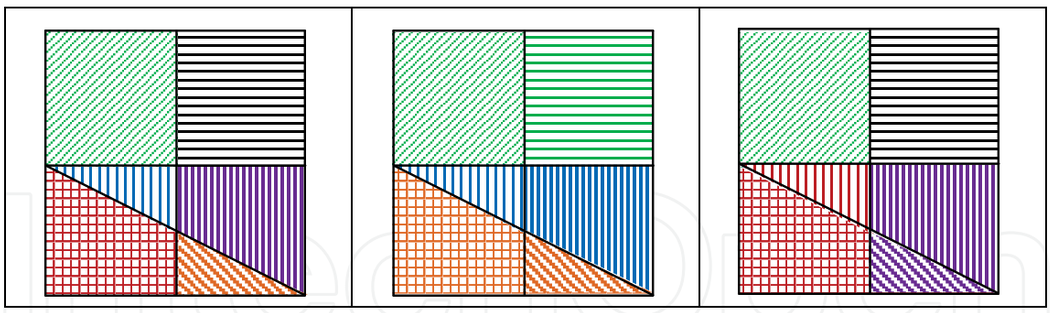
1. Introduction

The observation of a scene by an imaging sensor produces an image that is a function of the sensor characteristics and the sensor ability to interact with the targets in the scene. In this process the true classes in the scene can be merged or become very close in the image generated by the sensor in such way that each image, one for each sensor, can present different number of prevalent classes. As an example, Figure 1 shows a six classes scene that was observed by two sensors in two different ways. The first sensor generates an image that has three prevalent classes (green, blue and orange) and the second sensor generates an image with four prevalent classes (green, black, purple and red).

There are several mathematical approaches that can be used to classify the scene using one or more images of the scene. These approaches include Support Vector Machine (Bruzone et al., 2006; Camps-Valls et al., 2007), Artificial Intelligence (Liu et al., 2008), Decision Trees (Pal & Mather, 2003), New Nearest Neighbor Approaches (Zhu & Basir, 2005; Samaniego et al., 2008) and the most used statistical approach (Valet et al., 2001). In the context of the statistical classification, the Bayesian approach is widely used for the classification error mitigation (Fukunaga, 1990). In the statistical classification method based in the Maximum A Posteriori (MAP) the image set to be classified must contain all images with the same number and type of classes (Schowengerdt, 1997).

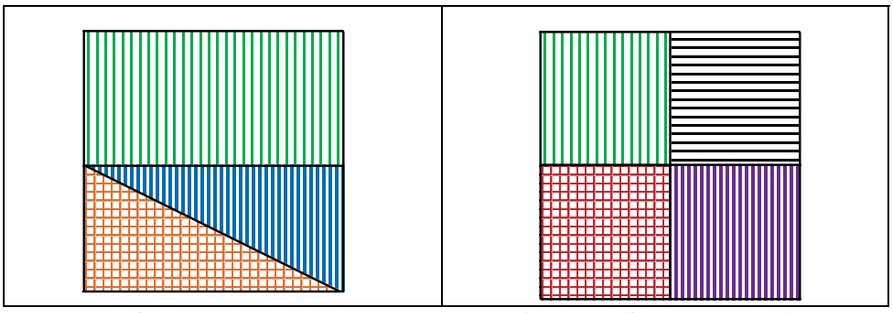
In this Chapter is presented an extension for the classical MAP classification for the case in which each image in a set of images can have different numbers and types of prevalent classes. In this extension, one image is chosen as the reference image to be classified according with its dominant classes and the others images are used as additional information (Maximo & Fernandes, 2008).

In the example shown in Figure 1 if the image 1 is selected as the reference image with three prevalent classes and image 2 as the complementary information, the perfect classification is given in Figure 2a. If the image 2 is selected as the reference, the ideal classification is given in the Figure 2b.



(a) Ground Truth (b) Image 1 (c) Image 2

Fig. 1. Classes definition: (a) Ground truth with six classes, (b) Three dominant classes (green, blue and orange) in the image generated by the first sensor and (c) Four dominant classes (green, black, purple and red) in the image generated by the second sensor



(a) Classification in 3 classes (b) Classification in 4 classes

Fig. 2. The ideal classification

In section 2 is presented the MAP classification and the proposed extension that consider one image in a set of images as the reference and that each image may have different numbers and types of prevalent classes. Section 3 shows the application of the proposed extended MAP classification method in comparison with the classical MAP classification by using simulated Single-Look Synthetic Aperture Radar (SLC-SAR) images (Oliver & Quegan, 1998). The classification performance comparison is due by the Kappa coefficient estimation (Rosenfield & Fitzpatrick-Lins, 1986).

2. The classification decision rule

2.1 The MAP decision rule

Given a set of N images where each image has M classes represented by w_m, m =1, 2,…M, the Bayes Risk is defined as (Sharf, 1991; Swain, 1978):

$$L_{\breve{x}}(w_m) = \sum_{k=1}^{M} \lambda_{km} p(w_k \mid \breve{x}) \tag{1}$$

where $\breve{x} = (x^{(1)}, x^{(2)}, \cdots, x^{(N)})$ is the observation set associated to the random variables (r.v.) $X = (X^{(1)}, X^{(2)}, \cdots, X^{(N)})$, with $X^{(n)}$ a r.v. representing a pixel in the n-th image, λ_{km} is the

classification loss function related to the observation $\breve{x}$ be classified in the class w_k when in the reality it belongs to the class w_m and $P(w_k \mid \breve{x})$ is the w_k class *a posteriori* probability (conditional probability after the observation). Choosing

$$\lambda_{km} = \begin{cases} 0 & \text{for} \quad k = m \\ 1 & \text{for} \quad k \neq m \end{cases} \tag{2}$$

the Bayes Risk becomes:

$$L_{\breve{x}}(w_m) = 1 - p(w_m \mid \breve{x}) \tag{3}$$

and the minimum Risk is reached when the *a posteriori* conditional probability is maximum. Then we can state a Maximum A Posteriori (MAP) decision rule as:

$$\breve{x} \mapsto w_m \Leftrightarrow F_m^o(\breve{x}) = F_k^o(\breve{x}) \tag{4}$$

where $\breve{x} \mapsto w_m$ represent the association of the observation $\breve{x}$ with the class w_m and $F_m^o(\breve{x})$ is the Global Membership Function (GMF) (Lee et al, 1987) given by:

$$F_m^o(\breve{x}) = P(w_m \mid \breve{x}) = \frac{P(w_m) p_X(\breve{x} \mid w_m)}{p_X(\breve{x})} \tag{5}$$

where $p_X(\breve{x} \mid w_m)$ is the probability density of X given that the w_m class is true (conditional probability). Since $p_X(\breve{x})$ is common to all GMF with m = 1,2,…, M, it can be neglected in the decision processes. Therefore the GMF can be simplified as

$$F_m^{os}(\breve{x}) = P(w_m) p_X(\breve{x} \mid w_m) \tag{6}$$

If we consider independent observations $p_X(\breve{x} \mid w_m) = \prod_{n=1}^{N} p_X(x^{(n)} \mid w_m)$ then

$$F_m^{os}(\breve{x}) = P(w_m) \prod_{n=1}^{N} p_X(x^{(n)} \mid w_m) \tag{7}$$

Equation (7) can be used in the decision rule as stated in (4) changing $F_m^o(\breve{x})$ to $F_m^{os}(\breve{x})$:

$$\breve{x} \mapsto w_m \Leftrightarrow F_m^{os}(\breve{x}) = F_k^{os}(\breve{x}) \tag{8}$$

2.2 The MAP decision rule for a reference image

It will be considered the general case in which every n-th image, n = 1, 2,…, N, has M_n classes represented by $w_{m_n}^{(n)}$, m_n=1, 2,…, M_n, and also that the first observation $x^{(1)}$ is the reference image, in the sense that we want to classify only the first image in its prevalent

classes and having the others images in the set as auxiliary or complementary information. In this case the Bayes Risk can be written as

$$L_{\breve{x}}(w_{m_1}^{(1)}) = \sum_{m_a=1}^{M_n} \lambda_{m_a m_1} p(w_{m_a}^{(1)} \mid \breve{x}) = 1 - p(w_k^{(1)} \mid \breve{x}) \tag{9}$$

and the decision rule by

$$x^{(1)} \mapsto w_{m_1}^{(1)} \Leftrightarrow F_{m_1}(\breve{x}) = F_{m_a}(\breve{x}) \tag{10}$$

where $F_{m_1}(\breve{x})$ is given by

$$F_{m_1}(\breve{x}) = P(w_{m_1}^{(1)} \mid \breve{x}) = \frac{p_X(\breve{x}, w_{m_1}^{(1)})}{p_X(\breve{x})} \tag{11}$$

Again $p_X(\breve{x})$ is independent of the class and can be neglected and the GMF $F_{m_1}(\breve{x})$ can be written as

$$\begin{aligned} F_{m_1}^s(\breve{x}) = p_X(\breve{x}, w_{m_1}^{(1)}) &= \sum_{m_2=1}^{M_2} \sum_{m_3=1}^{M_3} \dots \sum_{m_N=1}^{M_N} p_X(\breve{x}, w_{m_1}^{(1)}, w_{m_2}^{(2)}, \cdots, w_{m_n}^{(N)}) \\ &= \sum_{m_2=1}^{M_2} \sum_{m_3=1}^{M_3} \dots \sum_{m_N=1}^{M_N} p_X(\breve{x}, W_1^N) \\ &= \sum_{m_2=1}^{M_2} \sum_{m_3=1}^{M_3} \dots \sum_{m_N=1}^{M_N} p_X(\breve{x} \mid W_1^N) P(W_1^N) \\ &\overset{\text{Chain rule}}{=} P(w_{m_1}^{(1)}) \sum_{m_2=1}^{M_2} \sum_{m_3=1}^{M_3} \dots \sum_{m_N=1}^{M_N} p_X(\breve{x} \mid W_1^N) \prod_{n=2}^{N} P(w_{m_n}^{(n)} \mid W_1^{n-1}) \\ &\overset{\substack{\text{Independent} \\ \text{observations}}}{=} P(w_{m_1}^{(1)}) \sum_{m_2=1}^{M_2} \sum_{m_3=1}^{M_3} \dots \sum_{m_N=1}^{M_N} p_X(x^{(1)} \mid W_1^N) \prod_{n=2}^{N} p_X(x^{(n)} \mid W_1^N) P(w_{m_n}^{(n)} \mid W_1^{n-1}) \end{aligned} \tag{12}$$

where:

$$W_1^n = \left\{ w_{m_1}^{(1)}, w_{m_2}^{(2)}, \dots, w_{m_n}^{(n)} \right\} \tag{13}$$

Equation (13) can be used in the decision rule as stated in (10) changing $F_{m_1}(\breve{x})$ to $F_{m_1}^s(\breve{x})$:

$$x^{(1)} \mapsto w_{m_1}^{(1)} \Leftrightarrow F_{m_1}^s(\breve{x}) = F_{m_a}^s(\breve{x}) \tag{14}$$

In the particular case where all images have the same classes M_n=M and $w_m^{(n)} = w_m$ we have that $F_{m_a}^s(\breve{x}) = F_{m_a}^{os}(\breve{x})$.

We can define now the decision space $S_{m_1} \subset R$ in such way that

$$x^{(1)} \mapsto \omega_{m_1}^{(1)} \Rightarrow x^{(1)} \in S_{m_1} \tag{15}$$

2.3 The MAP decision rule for a set of classes

Let $\Psi_1^N(r_1, r_2, ..., r_N)$ be a set of any N classes, one class in each image, represented by

$$\Psi_1^N(r_1, r_2, ..., r_N) = \left\{ w_{m_1=r_1}^{(1)}, w_{m_2=r_2}^{(2)}, ..., w_{m_N=r_N}^{(N)} \right\}, \quad r_n \in \left\{ m_1, m_2, ...m_{M_n} \right\}, \quad n = 1, 2, ..., N \tag{16}$$

The classification of a pixel $\breve{x}$ in this special classes group can be made by the decision rule

$$\breve{x} \mapsto \Psi_1^N(r_1, r_2, ..., r_N) \Leftrightarrow F_{r_1, r_2, ..., r_N}(\breve{x}) = \max_{k_1, k_2, ...k_N} F_{k_1, k_2, ...k_N}(\breve{x}) \tag{17}$$

where the GMF function $F_{r_1, r_2, ..., r_N}(\breve{x})$ is given by:

$$\begin{aligned} F_{r_1, \cdots, r_N}(\breve{x}) &= p_X(\breve{x}, \Psi_1^N(r_1, r_2, ..., r_N)) = P(\Psi_1^N(r_1, r_2, ..., r_N)) p_X(\breve{x} \mid \Psi_1^N(r_1, r_2, ..., r_N)) \\ &= P(w_{r_1}^{(1)}) p_X(\breve{x} \mid \Psi_1^N(r_1, r_2, ..., r_N)) \prod_{n=2}^{N} p(w_{r_n}^{(n)} \mid \Psi_1^{n-1}(r_1, r_2, ..., r_{n-1})) \\ &\overset{\text{independent observations}}{=} p(w_{r_1}^{(1)}) p(x^{(1)} \mid \Psi_1^N(r_1, r_2, ..., r_N)) \prod_{n=2}^{N} p(x^n \mid \Psi_1^N(r_1, r_2, ..., r_N)) p(w_{r_n}^{(n)} \mid \Psi_1^{n-1}(r_1, r_2, ..., r_{n-1})) \end{aligned} \tag{18}$$

We can again define the decision space $S_{r_1, r_2, ..., r_N} \subset R^N$ in such way that

$$\breve{x} \mapsto \Psi_1^N(r_1, r_2, ..., r_N) \Rightarrow \breve{x} \in S_{r_1, r_2, ..., r_N} \tag{19}$$

The equation (18) can be introduced in (12) in such way that for independent images

$$F_{m_1}^s(\breve{x}) = \sum_{m_2=1}^{M_2} \sum_{m_3=1}^{M_3} ... \sum_{m_N=1}^{M_N} F_{m_1, ..., m_N}(\breve{x}) \tag{20}$$

The space $S_{m_1} \subset R$ in (15) and the space $S_{r_1, r_2, ..., r_N} \subset R^N$ in (19) are related by

$$S_{m_1} = \bigcap_{r_2=0}^{M_2} \bigcap_{r_3=0}^{M_3} ... \bigcap_{r_N=0}^{M_N} S_{m_1, r_2, ..., r_N} \tag{19}$$

The decision rule (10) and (19) can also be related by

$$x^{(1)} \mapsto w_{m_1}^{(1)} \Leftrightarrow \breve{x} \mapsto \Psi_1^N(m_1, r_2, ..., r_N), \quad r_n \in \left\{ m_2, ...m_{M_n} \right\}, \quad n = 2, ...N \tag{20}$$

An equivalent form of the decision rule (20) can be state as

$$x^{(1)} \in S_{m_1} \Leftrightarrow \breve{x} \in S_{m_1, r_2, \ldots, r_N}, \quad r_n \in \{m_2, \ldots m_{M_n}\}, \quad n = 2, \ldots N \tag{21}$$

Expression (20) can be generalized for any image k as a reference image, in such way that

$$F^s_{m_k}(\breve{x}) = \sum_{m_1=1}^{M_1} \sum_{m_2=1}^{M_2} \ldots \sum_{m_{k-1}=1}^{M_{k-1}} \sum_{m_{k+1}=1}^{M_{k+1}} \ldots \sum_{m_N=1}^{M_N} F_{m_1, m_2, \ldots m_{k-1}, m_{k+1}, \ldots, m_N}(\breve{x}) \tag{22}$$

and the decision rule becomes

$$x^{(k)} \mapsto w^{(k)}_{m_k} \Leftrightarrow F_{m_k}(\breve{x}) = \max_{m_a} F_{m_a}(\breve{x}), \quad k = 1, 2, \ldots, N \tag{23}$$

or in terms of decision space:

$$x^{(k)} \in S_{m_k} \Leftrightarrow \breve{x} \in S_{r_1, r_2, \ldots, r_{k-1}, m_k, r_{k+1}, \ldots, r_N}, \quad r_n \in \{m_1, m_2, \ldots, m_{k-1}, m_{k+1}, \ldots, m_{M_n}\}, \quad n = 2, \ldots N \tag{25}$$

with

$$S_{m_k} = \bigcap_{r1=0}^{M1} \bigcap_{r_2=0}^{M_2} \ldots \bigcap_{r_{k-1}=0}^{M_{k-1}} \bigcap_{r_{k+1}=0}^{M_{k+1}} \ldots \bigcap_{r_N=0}^{M_N} S_{r_1, r_2, \ldots, r_{k-1}, m_k, r_{k+1}, \ldots, r_N} \tag{26}$$

3. Simulation example

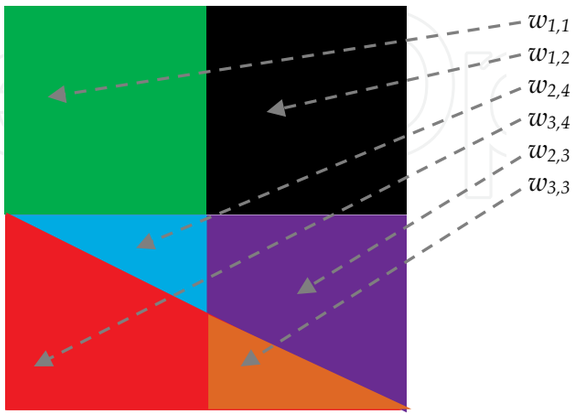
3.1 The simulated SAR images

Four set of two One-Look SAR images were simulated according to Table 1. The simulated SAR images have 512x512 pixels and are Rayleigh distributed (Oliver & Quegan, 1998). All of them have six classes and were smoothed by a *K*x*K* mean filter (*K* = 3, 5 and 7). The filtering causes that the distribution $p_X(x^{(n)} \mid w^{(1)}_{m_1}, w^{(2)}_{m_2}, \ldots w^{(N)}_{m_N})$ or $p_X(x^{(n)} \mid w^{(n)}_m)$ fit with a Gaussian distribution.

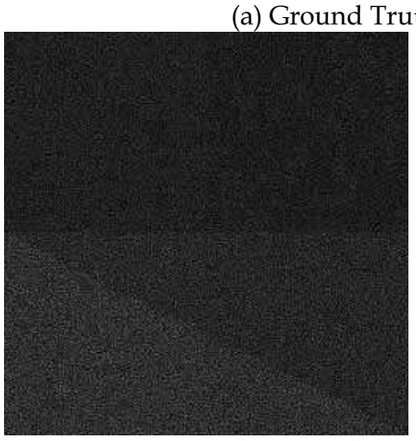
		Mean values of the Rayleigh r.v. for the classes					
Classes:		$w_{1,1}$	$w_{1,2}$	$w_{2,3}$	$w_{2,4}$	$w_{3,3}$	$w_{3,4}$
Set 1	Image 1a	20.6	19.4	24.4	25.6	29.4	30.6
	Image 2a	30	35	39.4	55.6	40.6	54.4
Set 2	Image 1a	20.6	19.4	24.4	25.6	29.4	30.6
	Image 2b	30	45	59	106	61	104
Set 3	Image 1b	21	19	34	36	49	51
	Image 2a	30	35	39.4	55.6	40.6	54.4
Set 4	Image 1b	21	19	34	36	49	51
	Image 2b	30	45	59	106	61	104

Table 1. Images sets with six classes parameters

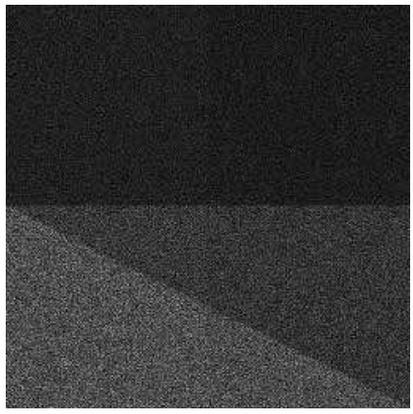
Figure 3(a) shows the ground truth of a scene with 6 classes with the labels: $w_{1,1}$, $w_{1,2}$, $w_{2,4}$, $w_{3,4}$, $w_{2,3}$ and $w_{3,3}$. The scene is observed by two different SAR sensors which generate two different and independent images with the mean values defined in Table 1. The different simulated images are shown in Figure 3(b)-3(e).



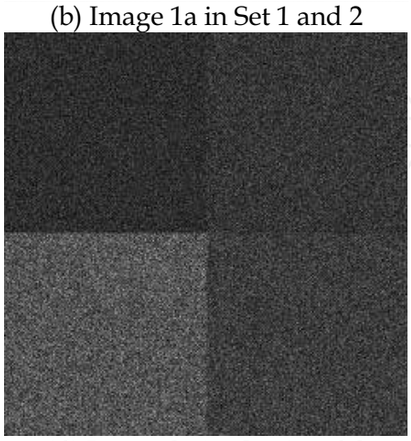
(a) Ground Truth with six classes



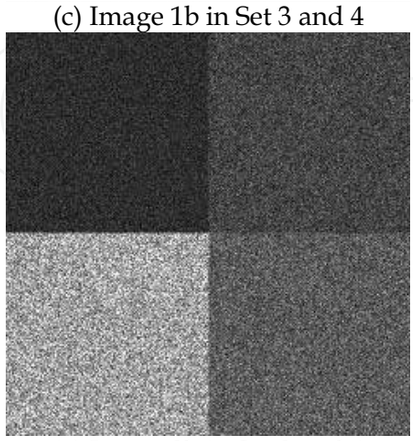
(b) Image 1a in Set 1 and 2



(c) Image 1b in Set 3 and 4



(d) Image 2a in Set 1 and 3



(e) Image 2b in Set 2 and 4

Fig. 3. Simulated SAR images with six classes

It is been considered that the sensors have some particular characteristics such that the first image generated by the sensor 1 (image 1a or 1b) has three prevalent classes and the second image (image 2a or 2b) generated by the sensor 2 has four classes. In all sets the Images 1a and 1b have three predominant classes each of them composed by two different classes:

$$\begin{aligned} w_1^{(1)} &= f_1^{(1)}(w_{1,1}, w_{1,2}) \\ w_2^{(1)} &= f_2^{(1)}(w_{2,3}, w_{2,4}) \\ w_3^{(1)} &= f_3^{(1)}(w_{3,3}, w_{3,4}) \end{aligned} \tag{27}$$

and in all sets the images 2a and 2b have four predominant classes each of them composed as follow:

$$\begin{aligned} w_1^{(2)} &= f_1^{(2)}(w_{1,1}) \\ w_2^{(2)} &= f_1^{(2)}(w_{1,2}) \\ w_3^{(2)} &= f_3^{(2)}(w_{2,3}, w_{3,3}) \\ w_4^{(2)} &= f_4^{(2)}(w_{2,4}, w_{3,4}) \end{aligned} \tag{28}$$

Image 1a has its predominant classes with the mean values of its components classes very close (difference equal to 1.2 - set 1 and 2). In image 1b the predominant classes are more separated (difference equal to 3.0 - set 3 and 4). Image 2a has its predominant classes with the mean values of its components classes very close (difference equal to 1.2 - set 1 and 3). In image 2b its predominant classes are more separated and more different (difference equal to 3.0 - set 2 and 4). Due to this simulated characteristics the classification become easier and therefore more precise from set 1 to set 4.
The *a priori* probabilities of the classes in the ground truth are given in Table 2 and the conditional probability is presented in Table 3.

Classes:	$w_{1,1}$	$w_{1,2}$	$w_{2,3}$	$w_{2,4}$	$w_{3,3}$	$w_{3,4}$
Probabilities:	1/4	1/4	3/16	1/16	1/16	3/16

Table 2. Six classes a priori probabilities

Classes:	m_2=1	m_2 =2	m_2 =3	m_2 =4
m_1 =1	1/2	1/2	0	0
m_1 =2	0	0	3/4	1/4
m_1 =3	0	0	1/4	3/4

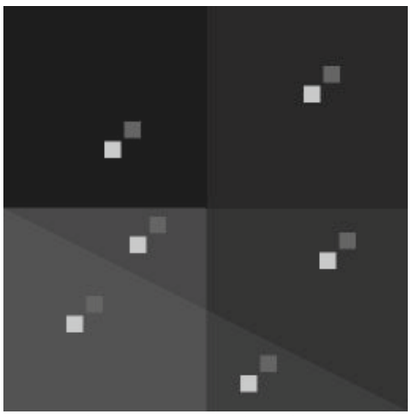
Table 3. Conditional probabilities $P(w_{m_1}^{(1)} \mid w_{m_2}^{(2)})$

3.2 The classification results

It was performed a supervised image classification of the six classes images in set 1, 2, 3 and 4 in three ways:

a) Image 1 was classified by equation (8) in six classes as a single image (N = 1);
b) Image 1 and 2 were classified in six classes by equation (8) as a bidimensional observation process (N = 2) and
c) Image 1 is selected as the reference image having the classes $w_1^{(1)}$, $w_2^{(1)}$ and $w_3^{(1)}$ and image 2 as the complementary image with the classes $w_1^{(2)}$, $w_2^{(2)}$, $w_3^{(2)}$ and $w_4^{(2)}$ in the classification structure given by equation (14).

In the supervised classification processes $p_X(x^{(1)}|W_1^N)$ and $p_X(x^{(n)}|W_1^{n-1})$ were estimated in a neighborhood of 20x20 pixels in each class and classes combinations. The error matrix (Congalton, 1991) for the Kappa estimation was also calculated in a different neighborhood also of 20x20 in each class. Figure 4 shows the samples used for the probability density estimations and for the error matrix calculation. The Kappa estimated values and its RMS error (Congalton & Green, 1999) considering the smooth filter with *K*x*K* = 3x3, 5x5 and 7x7 for the three classifications processes are shown in Tables 4 to 6.



(a) Estimation and test sample for the six classes classification



(b) Estimation and test samples for three classes classification

Fig. 4. Samples distributions in the images: ☐ estimation window and ▩ test window

The classification, as could be expected, is better with the use of the two images and become also better from the set 1 to 4. The classification performance considering the reference image is better than the others including the most critical situation that is given by the images in the set 1.

Classification in 6 classes (equat. 8)	Set 1	Set 2	Set 3	Set 4
Image 1	0.17±0.01	0.17±0.01	0.33±0.01	0.33±0.01
Image 1 and 2	0.32±0.01	0.51±0.01	0.53±0.01	0.71±0.01
Classification in 3 classes (equat. 14)	Set 1	Set 2	Set 3	Set 4
Reference Image 1	0.50±0.02	0.53±0.02	0.79±0.01	0.81±0.01

Table 4. Kappa values for the classification (3x3 smooth window)

Classification in 6 classes (equat. 8)	Set 1	Set 2	Set 3	Set 4
Image 1	0.26±0.01	0.26±0.01	0.43±0.01	0.43±0.01
Image 1 and 2	0.55±0.01	0.73±0.01	0.78±0.01	0.91±0.01
Classification in 3 classes (equat. 14)	Set 1	Set 2	Set 3	Set 4
Reference Image 1	0.74±0.02	0.78±0.01	0.94±0.01	0.96±0.01

Table 5. Kappa values for the classification (5x5 smooth window)

Classification in 6 classes (equat. 8)	Set 1	Set 2	Set 3	Set 4
Image 1	0.34±0.01	0.34±0.01	0.52±0.01	0.53±0.01
Image 1 and 2	0.73±0.01	0.84±0.01	0.90±0.01	0.98±0.01
Classification in 3 classes (equat. 14)	Set 1	Set 2	Set 3	Set 4
Reference Image 1	0.86±0.01	0.88±0.01	0.99±0.01	0.99±0.01

Table 6. Kappa values for the classification (7x7 smooth window)

Figures 5 and 6 show the classification results for the original SAR images smoothed by a 5x5 mean filter. In these figures it can be seen that the classification becomes better from the set 1 to 4 and the classification with the reference image get the best classification results.

3.3 The classification in three classes

We will now consider an extreme case in which the ground truth in Fig 3(a) has only three classes as shown in Fig 7(a) in such way that:

$$\begin{aligned} w_1 &= w_{1,1} \cup w_{1,2} \\ w_2 &= w_{2,3} \cup w_{2,4} \\ w_3 &= w_{3,3} \cup w_{3,4.} \end{aligned} \tag{29}$$

It is also considered the maximum possible classes separation in Table 1 resulting in images with Rayleigh r.v. mean values shown in Table 7. Figures 7(b)-7(e) show the four sets of images in the simulation.

The Kappa classification results using equation (8) with the smoothing filter wit KxK = 3x3, 5x5 and 7x7 are shown in Tables 8 - 10. The values in the last line of Tables 8 - 10 can be considered for each smooth filter as the limit value for the MAP classification in the ideal case for the simulated images. Comparing these values with the values in the last line of Tables 4 – 6, respectively, we conclude that for the worst case (set 1 and set 1o) the classification of the set 1 with a reference image has its Kappa:
75.8% of the value of the best classification in set 1o for 3x3 smooth window,
80.4% of the value of the best classification in set 1o for 5x5 smooth window, and
86.9% of the value of the best classification in set 1o for 7x7 smooth window.
Figures 8(a)-(c) and 9(a)-(c) show for the 5x5 smooth filter the classification results for the three classes images according to the images in the sets 1o, 2o, 3o and 4o. Figure 8(d)-(e) and Figure 9(d)-(e) repeat the three classes classification for the image 1a and 1b as reference images shown in Figure 5(d)-(e) and Figure 6(d)-(e), respectively.

		Mean values of the Rayleigh r.v. for the classes		
Classes:		w_1	w_2	w_3
Set 1o	Image 1oa	19.4	25.6	30.6
	Image 2oa	30	40.6	55.6
Set 2o	Image 1oa	19.4	25.6	30.6
	Image 2ob	30	61	106
Set 3o	Image 1ob	19	36	51
	Image 2oa	30	40.6	55.6
Set 4o	Image 1ob	19	36	51
	Image 2ob	30	61	106

Table 7. Images sets with three classes parameters

Classification in 3 classes: (equat. 8)	Set 1o	Set 2o	Set 3o	Set 4o
Image 1o	0.39±0.02	0.39±0.02	0.77±0.01	0.77±0.01
Image 1o and 2o	0.66±0.02	0.93±0.01	0.85±0.01	0.95±0.01

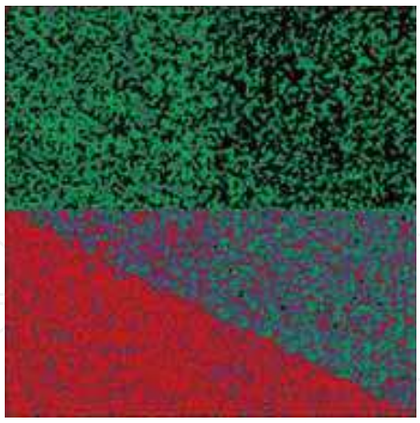
Table 8. Kappa values for the classification in three classes (3x3 smooth window)

Classification in 3 classes: (equat. 8)	Set 1o	Set 2o	Set 3o	Set 4o
Image 1o	0.61±0.02	0.61±0.02	0.93±0.01	0.93±0.01
Image 1o and 2o	0.92±0.01	0.99±0.01	0.98±0.01	0.99±0.01

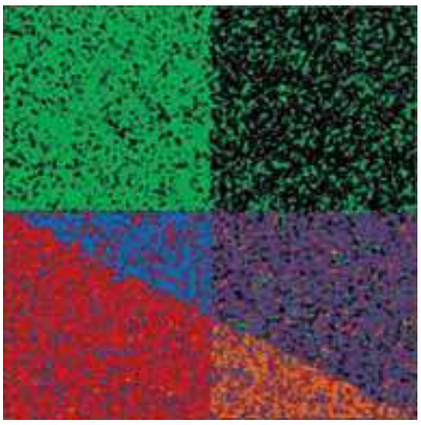
Table 9. Kappa values for the classification in three classes (5x5 smooth window)

Classification in 3 classes: (equat. 8)	Set 1o	Set 2o	Set 3o	Set 4o
Image 1o	0.81±0.02	0.81±0.01	0.99±0.01	0.99±0.01
Image 1o and 2o	0.99±0.01	1.00	1.00	1.00

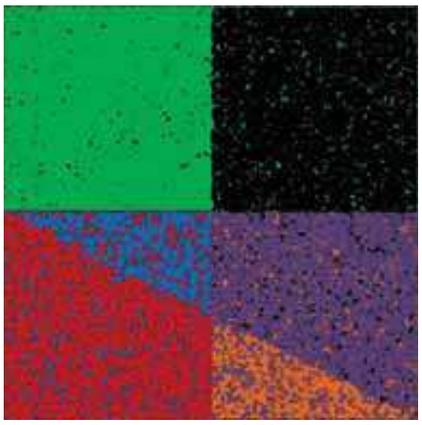
Table 10. Kappa values for the classification in three classes (7x7 smooth window)



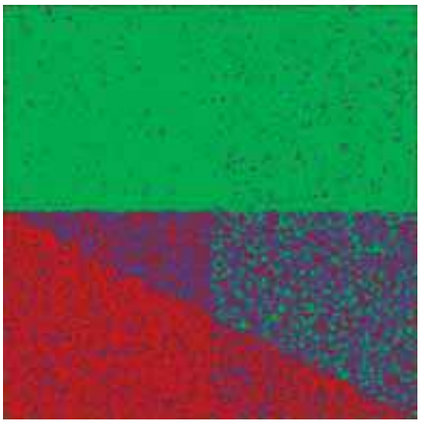
(a) Image 1a in set 1 and in set 2
Six classes classification



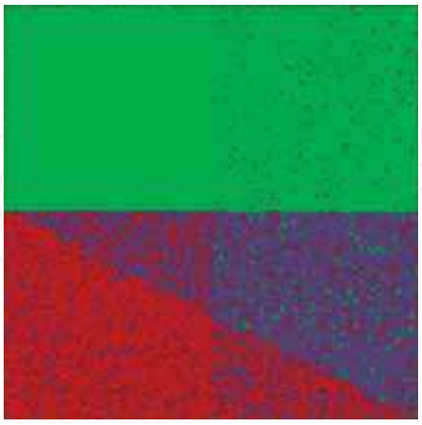
(b) Image 1a and 2a in set 1
Six classes classification



(c) Image 1a and 2b in set 2
Six classes classification



(d) Image 1a as reference in set 1
Three classes classification

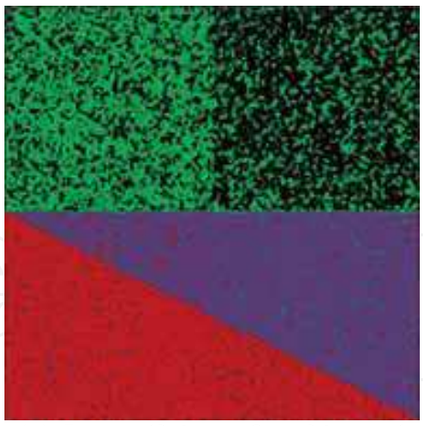


(e) Image 1a as reference in set 2
Three classes classification

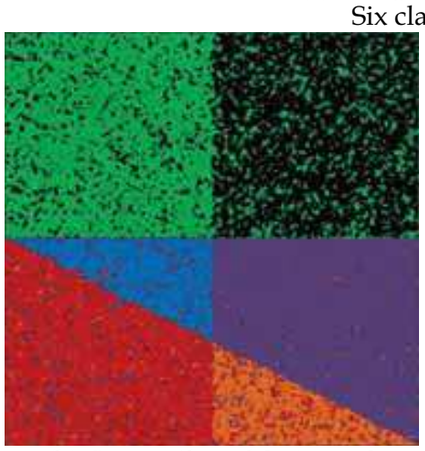
Six classes: $w_{1,1}$: $w_{1,2}$: $w_{2,3}$: $w_{2,4}$: $w_{3,3}$: $w_{3,4}$:

Three classes: $w_1^{(1)}$: $w_2^{(1)}$: $w_3^{(1)}$:

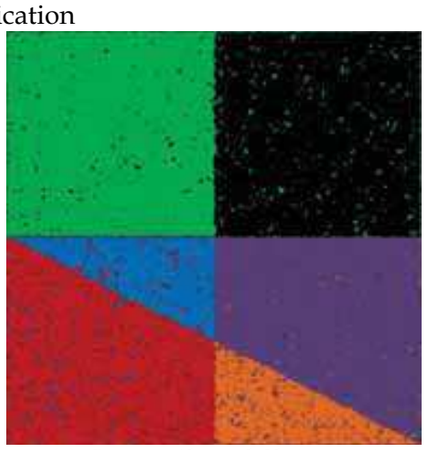
Fig. 5. Classification results in set 1 and set 2 (5x5 smooth filter)



(a) Image 1b in set 3 and in set 4
Six classes classification



(b) Image 1b and 2a in set 3
Six classes classification



(c) Image 1b and 2b in set 4
Six classes classification



(d) Image 1b as reference in set 3
Three classes classification

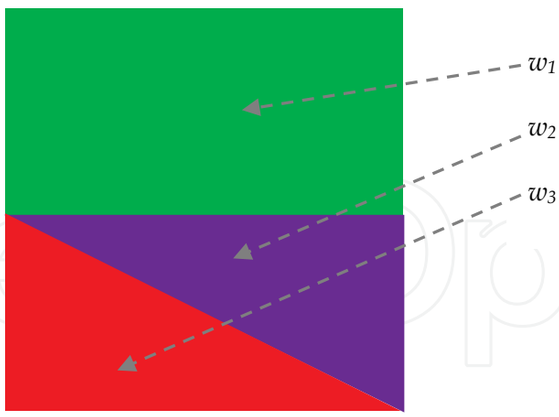


(e) Image 1b as reference in set 4
Three classes classification

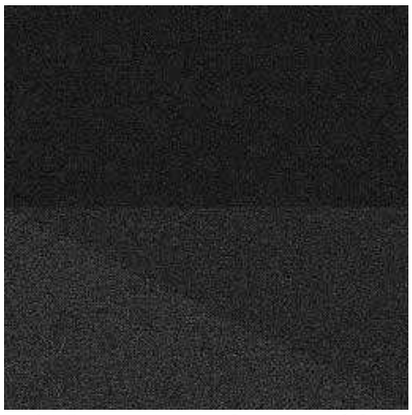
Six classes: $w_{1,1}$: $w_{1,2}$: $w_{2,3}$: $w_{2,4}$: $w_{3,3}$: $w_{3,4}$:

Three classes: $w_1^{(1)}$: $w_2^{(1)}$: $w_3^{(1)}$:

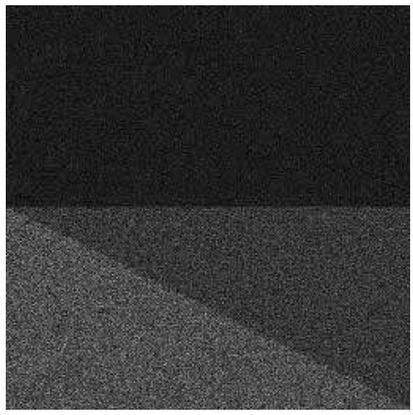
Fig. 6. Classification results in set 3 and set 4 (5x5 smooth filter)



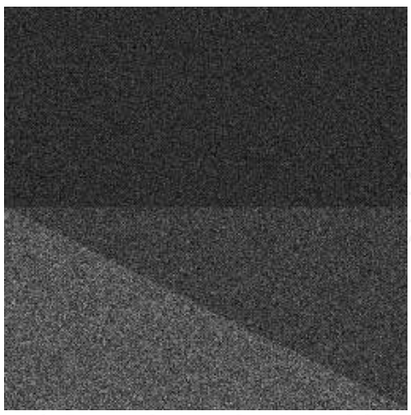
(a) Ground Truth with three classes



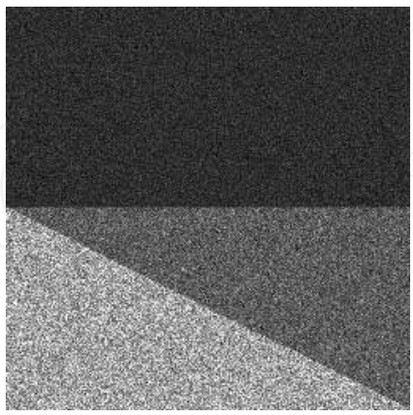
(b) Image 1oa in Set 1o and 2o



(c) Image 1ob in Set 3o and 4o

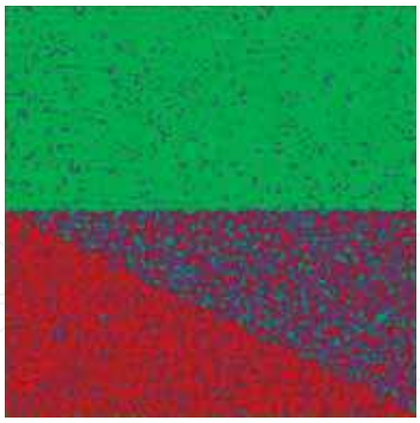


(d) Image 2oa in Set 1o and 3o



(e) Image 2ob in Set 2o and 4o

Fig. 7. Simulated images with three classes



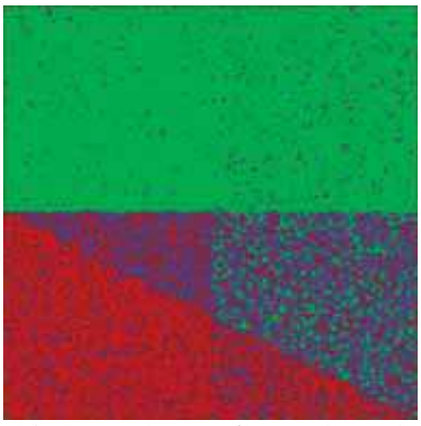
(a) Image 1oa in set 1o and in set 2o
Three classes classification



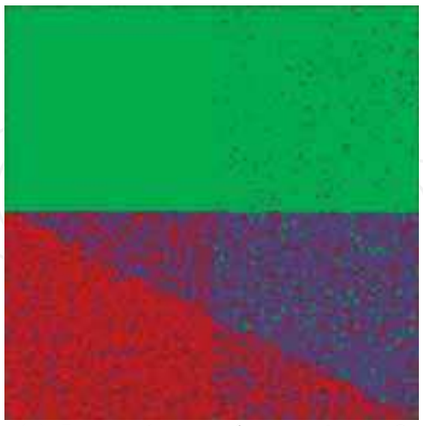
(b) Image 1oa and 2oa in set 1o
Three classes classification



(c) Image 1oa and 2ob in set 2o
Three classes classification



(d) Image 1a as reference in set 1
Three classes classification



(e) Image 1a as reference in set 2
Three classes classification

Three classes: $w_1^{(1)}$: $w_2^{(1)}$: $w_3^{(1)}$:

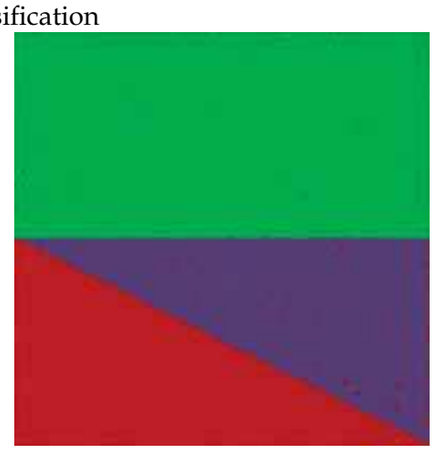
Fig. 8. Classification results in set 1o and set 2o (5x5 smooth filter)



(a) Image 1ob in set 3o and in set 4o
Three classes classification



(b) Image 1ob and 2oa in set 3o
Three classes classification



(c) Image 1ob and 2ob in set 4o
Three classes classification



(d) Image 1b as reference in set 3
three classes classification



(e) Image 1b as reference in set 4
three classes classification

Three classes: $w_1^{(1)}$: $w_2^{(1)}$: $w_3^{(1)}$:

Fig. 9. Classification results in set 3o and set 4o (5x5 smooth filter)

4. Conclusions

In the MAP classification context, it was shown a classification rule that consider a reference image to be classified and a set of complementary images as additional information. The images in the classification process can have different numbers and types of prevalent classes. The different prevalent classes are due to the imaging sensor characteristics (frequency, polarization, resolution etc) and its interaction with the scene (incidence angle, geometry, reflectivity etc).
It was presented a simulation example considering four sets of two amplitude SAR images of a scene. The reference and the complementary images have three and four dominant classes respectively. The original Rayleigh distributed images were filtered by a moving average filter and the new Gaussian distributed images had theirs parameters estimated for the MAP classification. The performance of the classification was evaluated by the error matrix Kappa coefficient.
In general, to apply the classification process that has a reference image to be classified and a set of images as complementary information one has to follow these steps to calculate the GMF $F^{s}_{m_1}(\breve{x})$ given by equation (12):

a) Each image, including the reference image, must be observed or raw classified in order to be established a raw map of all possible classes in the scene and in the images. In the presented simulation the scene has six classes $\{w_{1,1}, w_{1,2}, w_{2,3}, w_{2,4}, w_{3,3}, w_{3,4}\}$. The images have the classes $\{w_1^{(1)}, w_2^{(1)}, w_3^{(1)}\}$ and $\{w_1^{(2)}, w_2^{(2)}, w_3^{(2)}, w_4^{(2)}\}$ that are compositions of the former classes. The classes in each image and in the scene (considered as the ground truth) must have an association as shown in equations (27) and (28).

b) It must be estimated the *a priori* probability $P(w_{m_1}^{(1)})$ and the conditional probabilities, $P(w_{m_n}^{(n)} \mid W_1^{n-1})$ with $W_1^n = \left\{w_{m_1}^{(1)}, w_{m_2}^{(2)}, ..., w_{m_n}^{(n)}\right\}$. The classes $w_{m_n}^{(n)}$ that don't have an association with the classes in W_1^n, through the former classes in the scene, have as result $P(w_{m_n}^{(n)} \mid W_1^{n-1}) = 0$. In the simulation, the classes $w_1^{(1)} = f_1^{(1)}(w_{1,1}, w_{1,2})$ and $w_3^{(2)} = f_3^{(2)}(w_{2,3}, w_{3,3})$ don't have intersection and, therefore, $P(w_3^{(2)} \mid w_1^{(1)}) = 0$.

c) It must be estimated the conditional distribution parameters of $p_X(x^{(1)} \mid W_1^N)$ and $p_X(x^{(n)} \mid W_1^N)$ for all classes combinations that have intersections. In the simulation, the classes $w_1^{(1)}$ and $w_3^{(2)}$ don't have intersection and, therefore, $p_X(x^{(n)} \mid w_1^{(1)}, w_3^{(2)}) = 0$. If the images are not independent, the conditional distribution $p_X(\breve{x} \mid W_1^N)$ must be calculated instead $p_X(x^{(n)} \mid W_1^N)$.

d) Given $F^{s}_{m_1}(\breve{x})$ for each class $w_{m_1}^{(1)}$, m_1=1, 2,…, M_1, the decision rule (14) can be applied to classify only the reference image $x^{(1)}$ using the $x^{(2)}$, $x^{(3)}$,…, $x^{(N)}$ images as auxiliary information in the MAP decision processes.

5. References

Bruzone, L.;Chi, M. & Marconcini, M. (2006). A novel transductive svm for semisupervised classification of remote sensing images. *IEEE Transactions on Geoscience and Remote Sensing*, vol. 44, n. 11, November, pp. 3363-3373.

Camps-Valls, G.; Marsheva, T. & Zhou, D. (2007). Semi-supervised graph based hyperspectral image classification. *IEEE Transactions on Geoscience and Remote Sensing,* vol. 45, n. 10, October, pp. 3044-3054.

Congalton, R. & Green, K. (1999). *Assessing the accuracy of remotely sensed data: principles and practices*. Lewis Publishers, Boca Raton.

Congalton, R. (1991). A review of assessing the accuracy of classifications of remotely sensed data. *Remote Sensing of Environment*, vol. 37, n. 1, pp. 35-46.

Fukunaga, K. (1990). *Introduction to statistical pattern recognition, 2 ed.* Academic Press, San Diego.

Lee T.; Richards, J & Swain, P. H. (1987). Probabilistic and evidential approaches for multisource data analysis. *IEEE Transactions on Geoscience and Remote Sensing*, GE-25, n. 3, May, pp. 283-293.

Liu, X.; Li, X.; Liu, L.; He, J. & Ai, B. (2008). An innovative method to classify remote-sensing images using ant colony optimization. *IEEE Transactions on Geoscience and Remote Sensing*, vol. 46, n. 12, December, pp. 4198-4208.

Máximo, O. A. & Fernandes, D. (2009) *Classificação de imagens de diversas fontes de informação com o uso de controladores de influência para as imagens e suas classes* – PhD Thesis – Instituto Teconológico de Aeronáutica, Brasil – In Publishing Process.

Oliver, C. & Quegan, S (1998). *Understanding Synthetic Aperture Images*, Artech House, London.

Pal, M. & Mather, P. M. (2003). An assessment of the effectiveness of decision tree methods for land cover classification. *Remote Sensing of Environment*, vol. 86, pp. 554-565.

Rosenfield G. & Fitzpatrick-Lins, K. (1986). A coefficient of agreement as a measure of thematic classification accuracy. *Photogrammetric Engineering and Remote Sensing,* vol. 52, n. 2, February, pp. 223-227.

Samaniego, L.; Bárdossy, A. & Schulz, K. (2008). Supervised classification of remotely sensed imagery using a modified k-nn technique. *IEEE Transactions on Geoscience and Remote Sensing*, vol. 46, n. 7, July, pp. 2112-2125.

Schowengerdt, R. A. (1997) *Remote Sensing – Models and Methods for Image Processing*, Academic Press, San Diego.

Sharf, L. L. (1991). *Statistical signal processing – detection, estimation and time series analysis*. Addison-Wesley Publishing Company, Massachusetts.

Valet, L.; Mauris, G. & Bolon, P. (2001). A statistical overview of recent literature in information fusion. *IEEE Aerospace and Electronic Systems Magazine*, vol 16, n. 3, March, pp. 7-14.

Zhu, H. & Basir O. (2005). An adaptive fuzzy evidential nearest neighbor formulation for classifying remote sensing images. *IEEE Transactions on Geoscience and Remote Sensing*, vol. 43, n. 8, August, pp. 1874-1889.



Geoscience and Remote Sensing

Edited by Pei-Gee Peter Ho

ISBN 978-953-307-003-2
Hard cover, 598 pages
Publisher InTech
Published online 01, October, 2009
Published in print edition October, 2009

Remote Sensing is collecting and interpreting information on targets without being in physical contact with the objects. Aircraft, satellites ...etc are the major platforms for remote sensing observations. Unlike electrical, magnetic and gravity surveys that measure force fields, remote sensing technology is commonly referred to methods that employ electromagnetic energy as radio waves, light and heat as the means of detecting and measuring target characteristics. Geoscience is a study of nature world from the core of the earth, to the depths of oceans and to the outer space. This branch of study can help mitigate volcanic eruptions, floods, landslides ... etc terrible human life disaster and help develop ground water, mineral ores, fossil fuels and construction materials. Also, it studies physical, chemical reactions to understand the distribution of the nature resources. Therefore, the geoscience encompass earth, atmospheric, oceanography, pedology, petrology, mineralogy, hydrology and geology. This book covers latest and futuristic developments in remote sensing novel theory and applications by numerous scholars, researchers and experts. It is organized into 26 excellent chapters which include optical and infrared modeling, microwave scattering propagation, forests and vegetation, soils, ocean temperature, geographic information , object classification, data mining, image processing, passive optical sensor, multispectral and hyperspectral sensing, lidar, radiometer instruments, calibration, active microwave and SAR processing. Last but not the least, this book presented chapters that highlight frontier works in remote sensing information processing. I am very pleased to have leaders in the field to prepare and contribute their most current research and development work. Although no attempt is made to cover every topic in remote sensing and geoscience, these entire 26 remote sensing technology chapters shall give readers a good insight. All topics listed are equal important and significant.

How to reference

In order to correctly reference this scholarly work, feel free to copy and paste the following:

Orlando Alves Maximo and David Fernandes (2009). MAP Classification of a Reference Image Using Auxiliaries Images with Different Prevalent Classes, Geoscience and Remote Sensing, Pei-Gee Peter Ho (Ed.), ISBN: 978-953-307-003-2, InTech, Available from: http://www.intechopen.com/books/geoscience-and-remote-sensing/map-classification-of-a-reference-image-using-auxiliaries-images-with-different-prevalent-classes

INTECH
open science | open minds

InTech Europe
University Campus STeP Ri
Slavka Krautzeka 83/A

InTech China
Unit 405, Office Block, Hotel Equatorial Shanghai
No.65, Yan An Road (West), Shanghai, 200040, China

www.intechopen.com

51000 Rijeka, Croatia
Phone: +385 (51) 770 447
Fax: +385 (51) 686 166
www.intechopen.com

中国上海市延安西路65号上海国际贵都大饭店办公楼405单元
Phone: +86-21-62489820
Fax: +86-21-62489821

IntechOpen

IntechOpen

© 2009 The Author(s). Licensee IntechOpen. This chapter is distributed under the terms of the Creative Commons Attribution-NonCommercial-ShareAlike-3.0 License, which permits use, distribution and reproduction for non-commercial purposes, provided the original is properly cited and derivative works building on this content are distributed under the same license.

IntechOpen

IntechOpen